Chapter 3

Spin-Fluctuation-Mediated Effective Interaction

The Hubbard model is a fundamental model in solid state physics. It is used to study metallic ferromagnetism, metal-insulator transitions (the Mott transition), high-T_c superconducting cuprates and so on. It is also an appropriate model for liquid ^{3}He. In this chapter we study the two-dimensional (2D) Hubbard model as a model for 2D liquid ^{3}He.

It is well know that, in 3D liquid ^{3}He, p-wave superfluidity is caused by strong ferromagnetic spin fluctuations [1, 2, 3, 4, 5]. In 2D, the uniform magnetic susceptibility is also strongly enhanced in the dense region as in 3D [6]. One can therefore expect that spin fluctuations induce superfluidity in 2D, too. If this is the case, one of the fundamental questions is symmetry of Cooper pairs.

The symmetry of the Cooper pairs formed by spin-fluctuation-mediated interaction is mainly determined by the wave number dependence of the magnetic susceptibility [1, 2, 3, 4, 5]. In 3D, the susceptibility of a non-interacting fermion system has a maximum at $q = 0$. When one introduces short-ranged repulsive interaction between fermions and treats it with the random phase approximation (RPA), one finds that the peak at $q = 0$ is the most strongly enhanced. Even if one further considers correlation effects, effects not included in the RPA, it is likely that the susceptibility still has the strong maximum at $q = 0$. This nearly ferromagnetic susceptibility leads to the p-wave superfluidity.

In 2D, the susceptibility of non-interacting fermions is independent of the wave number as far as the wave number is less than twice the fermi wave number, $q < 2k_F$. In the RPA, this is also true when the wave number dependence of interaction is neglected. One then finds that spin fluctuations generate no effective attractive interaction between a fermion with momentum $\boldsymbol{k}_F$ and a fermion with momentum

$-k_F$ in the static limit.

In contrast to 3D, correlation effects can qualitatively change the wave number dependence of the susceptibility in 2D . It is therefore important to study the correlation effects on the spin susceptibility to discuss the effective interaction mediated by spin fluctuations and superfluidity possibly caused by it.

The main purpose of this chapter is to study the wave number dependence of the static spin susceptibility and the effective interaction for Cooper problem in the dilute 2D Hubbard model. Using the quantum Monte Carlo method [7] and a propagator-renormalized perturbation theory [8, 9], we study the spin susceptibility in the strongly correlated region. To make results directly relevant to 2D liquid ^{3}He, the calculations are restricted to the dilute limit where lattice effect is negligible. It should be noted that results obtained in this study can also be applied to 2D electron gas.

3.1 Formulation

3.1.1 Model Hamiltonian

The 2D Hubbard Hamiltonian on the square lattice has the following form in momentum representation:

$$\begin{aligned} \mathcal{H}^{(Eff)} &= \sum_{\boldsymbol{k},\sigma} \xi_{\boldsymbol{k}} a^{\dagger}_{\boldsymbol{k}\sigma} a_{\boldsymbol{k}\sigma} \\ &+ \frac{U}{N} \sum_{\boldsymbol{k},\boldsymbol{k}'} \sum_{\boldsymbol{q}} a^{\dagger}_{\boldsymbol{k}-\boldsymbol{q}\uparrow} a^{\dagger}_{\boldsymbol{k}'+\boldsymbol{q}\downarrow} a_{\boldsymbol{k}'\downarrow} a_{\boldsymbol{k}\uparrow}, \end{aligned} \tag{3.1}$$

where $a_{\boldsymbol{k}\sigma}(a^{\dagger}_{\boldsymbol{k}\sigma})$ is the annihilation(creation) operator for fermions of momentum $\boldsymbol{k}$ and spin σ, $\xi_{\boldsymbol{k}} = -2t(\cos(k_x a) + \cos(k_y a)) - \mu$, a is the lattice constant, t is the hopping energy between the nearest neighbor sites, μ is the chemical potential, U is the on-site repulsion, and N is the total number of the lattice points.

Near the bottom of the band, the spectrum $\xi_{\boldsymbol{k}}$ is approximated as

$$\xi_{\boldsymbol{k}} = \frac{1}{2m_3} k^2 - \mu - 4t, \tag{3.2}$$

where $m_3 = \frac{1}{2ta^2}$. Therefore, in the dilute limit, $n \ll 1$, where n is the number of fermions per lattice point, effect of lattice is negligible.

3.1.2 QMC

Using the grand canonical quantum Monte Carlo method [7] (See Appendix 3.A), the static spin susceptibility of the 2D Hubbard model in the dilute limit is calculated. The QMC approach has the potential to treat strongly correlated systems, allowing us to go far beyond approximate methods, e.g., a perturbation method. It provides numerically exact results and yields reliable information about strongly correlated systems over a vast parameter range.

At low temperatures, the grand canonical QMC algorithm [7] becomes increasingly useless not only because the numerical effort to go to lower temperatures itself increases the computer time, but also because numerical instabilities start to dominate at low temperatures. These numerical instabilities are suppressed by a Gram-Schmidt scheme; the instabilities and the scheme to avoid them are discussed in detail in refs. 7 and 10.

Another possible obstacle to go down to low temperatures is the "negative sign" problem. In the dilute limit, the "negative sign" problem is not so serious. Actually, in this study, we do not go down to the low-temperature regime where the "negative sign" problem becomes serious, because finite size effects become too large for the results to be reliable before the "negative sign" problem gets serious. In the present simulations, the probability distribution is almost positive-semidefinite.

The QMC provides us primarily with one-particle Green's functions (in imaginary time)

$$G_\sigma(i,\tau;j,\tau') = -\langle T_\tau a_{i\sigma}(\tau) a^\dagger_{j\sigma}(\tau')\rangle, \tag{3.3}$$

and two-particle Green's functions,

$$\begin{aligned} &G^{(2)}_\sigma(i,\tau_1,j,\tau_2;i',\tau_1' j',\tau_2') \\ &= \langle T_\tau a_{i\sigma}(\tau_1) a_{j\sigma}(\tau_2) a^\dagger_{j'\sigma}(\tau_2') a^\dagger_{i'\sigma}(\tau_1')\rangle. \end{aligned} \tag{3.4}$$

Equations (3.3) and (3.4) can be used to compute observables such as the susceptibility. The static spin susceptibility $\chi(q)$ is defined as

$$\chi(q) = \int_0^{1/T} \mathrm{d}\tau \left\langle T_\tau S^z_q\ (\tau) S^z_{-q}\ (0)\right\rangle, \tag{3.5}$$

where S^z_q is given by

$$S^z_q = \mu_0 \sum_k \left[a^\dagger_{q+k,\uparrow} a_{k,\uparrow} - a^\dagger_{q+k,\downarrow} a_{k,\downarrow}\right].$$

Here μ_0 is the magnetic moment. The magnetic unit is fixed as $\mu_0 = 1$.

In the Monte Carlo sampling procedure, we take $2 \times 10^4 \sim 8 \times 10^4$ Monte Carlo samples, divide the samples into 10 groups (bins), and then measure the standard deviation among the 10 bins. The standard deviation is shown by an error bar in the following figures.

3.1.3 Conserving approximations

Self-energy

We also study the susceptibility of the dilute Hubbard model using a propagator-renormalized perturbation theory (conserving approximations [8]) for the temperature Green's function. This method gives access to remarkably larger lattice sizes. As a consequence, it provides good access to very low temperatures, which is difficult to treat by the QMC due to severe finite size effects.

This method may be generated by following an approach introduced by Baym and Kadanoff [8]: (1) first, write down a free-energy functional Φ in terms of the dressed single-particle Green's function G and the interaction U, (2) generate an approximation for the single-particle selfenergy Σ by functional differentiation of Φ with respect to G, and (3) compute G self-consistently using this selfenergy. The essence and the complexity are hidden in the functional $\Phi[G]$, which is usually approximated by some infinite subset of the one-particle irreducible Feynman diagrams.

We take for $\Phi[G]$ the following four sorts of diagrams (see Figs. 1(a)-1(c)). (1) $\Phi^{(2)}$: diagrams describing the full contributions of $O(U^2)$. (2) $\Phi^{(ph)}$: diagrams describing the full contributions of particle-hole scattering [9]. These diagrams represent spin fluctuations and charge fluctuations. (3) $\Phi^{(pp)}$: diagrams describing the full contributions of particle-particle scattering. (4) $\Phi^{(ph+pp)}$: diagrams describing the full contributions of particle-hole scattering and particle-particle scattering. We shall hereafter refer to the approach with $\Phi^{(2)}$ as the second order perturbation theory (SOPT), the approach with $\Phi^{(ph)}$ as the fluctuation exchange approximation (FLEX) [9] and the approach with $\Phi^{(pp)}$ as the (self-consistent) T-matrix approximation.

Each free-energy functional $\Phi^{(*)}$ ($*$ represents 2, ph, pp or $ph+pp$) is expressed in terms of G and U as follows:

$$\Phi^{(2)} = -\frac{1}{2}\mathrm{Tr}[(U\pi_{ph})^2], \tag{3.6}$$

$$\Phi^{(ph)} = \Phi^{(ph,s)} + \Phi^{(ph,c)} + \Phi^{(2)}, \tag{3.7}$$

$$\Phi^{(ph,s)} = \frac{3}{2}\mathrm{Tr}[\ln(1 - U\pi_{ph}) + U\pi_{ph} + \frac{1}{2}(U\pi_{ph})^2], \tag{3.8}$$

$$\Phi^{(ph,c)} = \frac{1}{2}\mathrm{Tr}[\ln(1+U\pi_{ph}) - U\pi_{ph} + \frac{1}{2}(U\pi_{ph})^2], \tag{3.9}$$

$$\Phi^{(pp)} = \mathrm{Tr}[\ln(1+U\pi_{pp}) - U\pi_{pp} + \frac{1}{2}(U\pi_{pp})^2] + \Phi^{(2)}, \tag{3.10}$$

and

$$\Phi^{(ph+pp)} = \Phi^{(ph)} + \Phi^{(pp)} - \Phi^{(2)}, \tag{3.11}$$

where the particle-hole bubble $\pi_{ph}(q)$ and the particle-particle bubble $\pi_{pp}(q)$ are defined by

$$\pi_{ph}(q) = -\sum_k G(q+k)G(k), \tag{3.12}$$

$$\pi_{pp}(q) = \sum_k G(q-k)G(k), \tag{3.13}$$

respectively. The used abbreviations is $\mathrm{Tr}[A] = \frac{T}{N}\sum_{\boldsymbol{k}}\sum_{\mathrm{i}\varepsilon_n} A(\boldsymbol{k}, \mathrm{i}\varepsilon_n)$.

The selfenergy $\Sigma^{(*)}$ is obtained by functional differentiation of $\Phi^{(*)}$ with respect to the Green's function G. The second order selfenergy $\Sigma^{(2)}$is given as follows:

$$\Sigma^{(2)}(k) = \sum_q \left[G(k-q)V^{(2)}(q)\right], \tag{3.14}$$

$$V^{(2)}(q) = U^2\pi_{ph}(q). \tag{3.15}$$

Similarly, $\Sigma^{(ph)}$is given as follows:

$$\Sigma^{(ph)}(k) = \sum_q \left[G(k-q)V^{(ph)}(q)\right], \tag{3.16}$$

where

$$V^{(ph)}(q) = \frac{3}{2}U^2\Pi_s(q) + \frac{1}{2}U^2\Pi_c(q) - U^2\pi_{ph}(q), \tag{3.17}$$

$$\Pi_s(q) = \frac{\pi_{ph}(q)}{1-U\pi_{ph}(q)}, \tag{3.18}$$

and

$$\Pi_c(q) = \frac{\pi_{ph}(q)}{1+U\pi_{ph}(q)}. \tag{3.19}$$

$\Sigma^{(pp)}$is given as follows:

$$\Sigma^{(pp)}(k) = \sum_q \left[G(-k+q)V^{(pp)}(q)\right], \tag{3.20}$$

where

$$V^{(pp)}(q) = -U^2\frac{\pi_{pp}(q)}{1+U\pi_{pp}(q)}, \tag{3.21}$$

and $\Sigma^{(ph+pp)}$is given as follows:

$$\Sigma^{(ph+pp)}(k) = \sum_q \left[G(-k+q) V^{(ph+pp)}(q) \right], \tag{3.22}$$

where

$$V^{(ph+pp)}(q) = V^{(ph)}(q) + V^{(pp)}(q) - V^{(2)}(q). \tag{3.23}$$

The Green's function G is expressed in terms of the selfenergy Σ as

$$G(k) = \left(\mathrm{i}\varepsilon_n - \varepsilon_{\boldsymbol{k}} - \Sigma(k) \right)^{-1}. \tag{3.24}$$

Equation (3.14) (, (3.16), (3.20) or (3.22)) and Eq. (3.24) then constitute self-consistent equations.

When we carry out summations over the momentum and the Matsubara frequency in the numerical calculation, the first Brillouin zone (FBZ) is divided into fine meshes and the frequency summation is terminated at a cut-off energy ω_c. The frequency cut-off ω_c is chosen to be $160t$, which we find to be sufficiently large. We solve the self-consistent equations using the Fast Fourier transformation (FFT) [11]. The FFT is very efficient when the frequency and momentum summations are convolutions, as in the present case.

Susceptibility

In order to calculate the static spin susceptibility $\chi(q)$ within conserving approximations [8], it is necessary to compute the vertex corrections. The proper polarization propagator $P_{\sigma_1\sigma_2\sigma_3\sigma_4}(q)$ is a set of the diagrams which do not split into two distinct diagrams when one interaction line is cut. In terms of the proper polarization propagator, $\chi(q)$ is given by

$$\chi(q) = \frac{2P_-(q)}{1 - UP_-(q)}, \tag{3.25}$$

where $P_-(q) = P_{\uparrow\uparrow\uparrow\uparrow}(q) - P_{\uparrow\downarrow\downarrow\uparrow}(q)$ (the subscripts $\uparrow\uparrow\uparrow\uparrow$ and $\uparrow\downarrow\downarrow\uparrow$ indicate the relative spins of the initial-state particle-hole pair and the final-state one, and the subscript $-$ indicates $O_- = O_{\uparrow\uparrow\uparrow\uparrow} - O_{\uparrow\downarrow\downarrow\uparrow}$.).

The proper polarization propagator $P_-$is given by

$$P_-(q) = -\sum_k G(q+k) G(k) K_-(q;k), \tag{3.26}$$

in terms of the three-point vertex function $K_-(q;k)$. The three-point vertex function $K_-(q;k)$ satisfies the integral equation

$$K_-(q;k) = 1 + \sum_{k'} \gamma_-(q;k,k') G(q+k') G(k') K_-(q;k'), \tag{3.27}$$

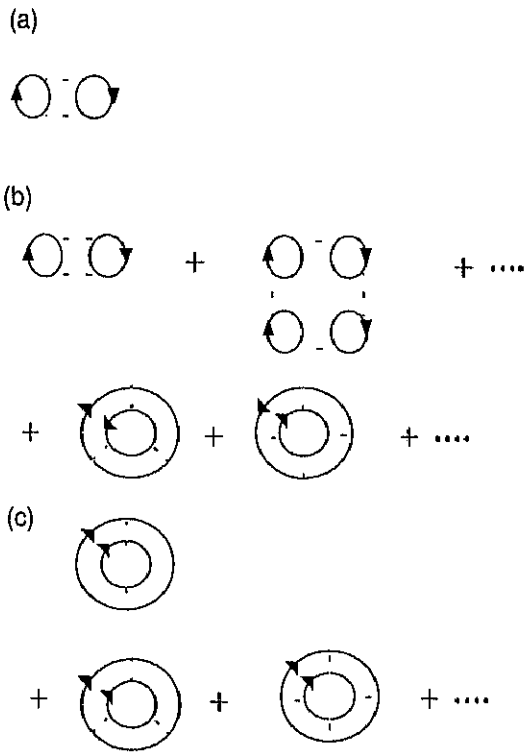

Figure 3.1: Diagrams representing a free energy functional $\Phi[G]$ in conserving approximations for the Hubbard model. The dashed line represents the interaction U and the solid line represents the Green's function G. (a) $\Phi^{(2)}$ diagrams, (b) $\Phi^{(ph)}$ diagrams, and (c) $\Phi^{(pp)}$ diagrams.

where $\gamma_-(q;k,k')$ is the irreducible four-point vertex function. If the irreducible four point-vertex function $\gamma_-(q;k,k')$ is given in terms of G and U, one can calculate the three-point vertex function $K_-(q;k)$ by solving Eq. (3.27).

In general the functional differentiation of the selfenergy $\Sigma^{(*)}$ generates two sorts of contributions to the irreducible vertex $\gamma^{(*)}(q;k,k')$ for the particle-hole scattering: one is expressed as diagrams where one fluctuation propagator is exchanged. The other is expressed as diagrams where the initial state particle-hole pair is converted into two fluctuation propagators and then recombined into the final state pair. We call the first set of contributions Maki-Thompson (MT) diagrams and the second Aslamasov-Larkin (AL) diagrams for convenience [12, 13, 14]. AL diagrams are shown in Appendix 3.B. AL diagrams are expensive to calculate in comparison with MT diagrams because the FFT algorithm cannot be applied to AL diagrams. We have confirmed that the contributions of AL diagrams are negligibly small in a small lattice, $N = 8\times 8$ [15]. In this study the contributions from AL diagrams are simply neglected in lager lattices. The irreducible four-point vertex $\gamma_-^{(*)}$ are then given by (See Fig. 3.2(a)- Fig. 3.2(c).)

$$\gamma_-^{(2)}(q;k,k') = U^2\pi_{pp}(q+k+k'), \tag{3.28}$$

$$\gamma_-^{(ph)}(q;k,k') = \frac{U^2}{2}(\Pi_c(k-k') - \Pi_s(k-k')), \tag{3.29}$$

$$\gamma_-^{(pp)}(q;k,k') = \frac{U^2\pi_{pp}(q+k+k')}{1+U\pi_{pp}(q+k+k')}, \tag{3.30}$$

$$\gamma_-^{(ph+pp)}(q;k,k') = \gamma_-^{(ph)} + \gamma_-^{(pp)}. \tag{3.31}$$

We give further discussions on the effect of vertex corrections in Appendixes 3.B and 3.C.

3.1.4 Effective interaction

We estimate the effective interaction between quasiparticles mediated by spin fluctuations by using a paramagnon theory [1]. We consider the effective interaction between two quasiparticles on the fermi surface with zero total momentum. The effective interaction is then separated into the triplet channel and the singlet channel. In the static limit, the interaction in the triplet channel is given by

$$v_t(k,k') = -\frac{U^2}{8}\left[\chi(k-k') - \chi(k+k')\right], \tag{3.32}$$

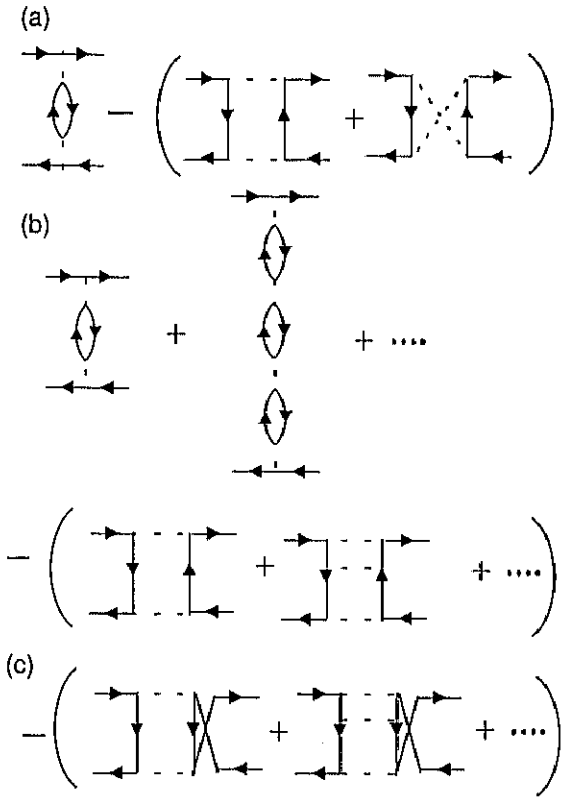

Figure 3.2: Diagrams representing the irreducible four-point vertex function. (a) $\gamma_{-}^{(2)}$ diagrams, (b) $\gamma_{-}^{(ph)}$ diagrams and (c) $\gamma_{-}^{(pp)}$ diagrams

where k and $-k$ are momenta of incoming fermions and k' and $-k'$ are those of outgoing fermions ($|k| = |k'| = k_F$). Similarly, the effective interaction in the singlet channel is given by

$$v_s(k,k') = \frac{3U}{2} + \frac{3U^2}{8}[\chi(k-k') + \chi(k+k')]. \tag{3.33}$$

In obtaining Eq. (3.32) and Eq. (3.33), the wave function renormalization is neglected for simplicity. Moreover, a part of the diagrams describing the effective interaction is neglected. This neglect may be justified when the spin susceptibility is strongly enhanced (See Appendix 3.D.).

To see the symmetry of the Cooper pair formed by the interaction (3.32) or (3.33), we have to expand the interaction with the eigenfunctions of the angular momentum m as was done in §2.1.2. In 2D, the strength λ_m of the interaction in the channel with angular momentum m is given by

$$\lambda_m = \frac{1}{2\pi}\int_0^{2\pi} \mathrm{d}\theta_{k\cdot k'} \cos(m\theta_{k\cdot k'}) v_\mu(k,k'), \tag{3.34}$$

where μ represents t or s, and $\theta_{k\cdot k'}$ is the angle between k and k'. Negative λ_m represents attractive interaction in the channel with angular momentum m.

3.2 Results

3.2.1 QMC

In this subsection, we show the results obtained with the QMC. Here and in the following we put $t = 1$ and $a = 1$. Except where otherwise noted, calculations in §3.2.1 and §3.2.2 are done at $T = 0.5$ and $n = 0.186$. Since the fermi energy ε_F for $U = 0$ at $n = 0.186$ is given by $\varepsilon_F = 0.96$, $\frac{T}{\varepsilon_F} = 0.52$. Furthermore, we show the results obtained using the Trotter number $L = \frac{8}{T}(\Delta\tau = \frac{1}{TL} = \frac{1}{8})$. We find that the systematic error from a finite Trotter number is negligible in the parameter regime studied in this thesis. In Fig. 3.3, we show the static spin susceptibility $\chi(q)$ at $T = 0.5$ and $U = 12$ for three different lattice size: $N = 6\times 6, 8\times 8$ and 10×10. It can be seen that the size with 8×8 is sufficient at this temperature. In the following, therefore, we present the results for $N = 8\times 8$.

We show the static spin susceptibility $\chi(q)$ for different values of U in Fig. 3.4. The wave vector q is in the diagonal direction in the first Brillouin zone. It can be seen that as U become large, the susceptibility $\chi(q)$ is enhanced, in particular, at $q = 0$, and a maximum develops at $q = 0$. This implies that the wave number dependence becomes ferromagnetic due to strong correlation.

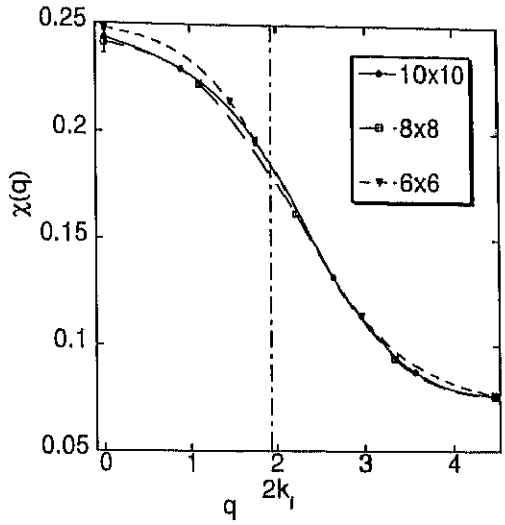

Figure 3.3: The static spin susceptibility $\chi(q)$ obtained with the QMC at $U = 12$ and $T = 0.5$ for variety of lattice size. The vertical dashed-dotted line stands for the location of $q = 2k_F$.

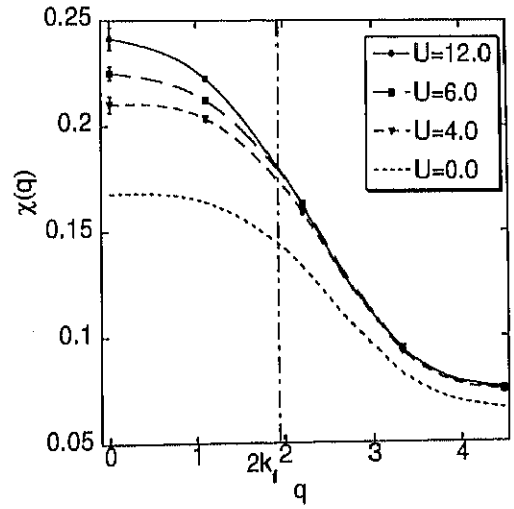

Figure 3.4: The wave number dependence of the static spin susceptibility $\chi(q)$ obtained with the QMC at $T = 0.5$ and $N = 8 \times 8$ for various values of U.

Next we investigate the temperature dependence of $\chi(q)$. As seen in Fig. 3.5, the ferromagnetic structure (i.e., a maximum at $q = 0$) is not visible at higher temperature than $T = 0.6$ and it emerges as temperature is lowered. If the ferro-

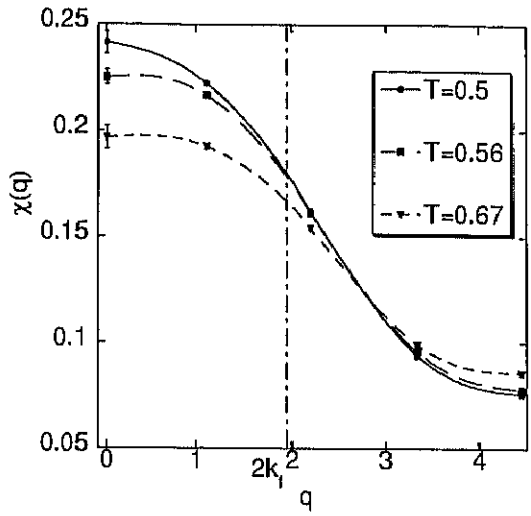

Figure 3.5: The static spin susceptibility $\chi(q)$ for three different temperatures at $U = 12$ and $N = 8 \times 8$.

magnetic structure were owing to the finite temperature effect, it would diminish as temperature is lowered. From this observation, we conclude that the wave number dependence of $\chi(q)$ becomes ferromagnetic due to the strong correlation. At lower temperatures than $T = 0.5$, it is expected that the enhancement around $q = 0$ becomes more prominent. The finite size effect becomes so severe, however, that reliable results cannot be obtained with the QMC at these temperatures.

3.2.2 Comparison of the QMC with the FLEX

To study $\chi(q)$ at low temperatures, we have to resort to approximations. It is not obvious what is the best approximation, say, among those mentioned in §3.1.3. In this subsection, therefore, we choose the most appropriate approximation by comparing approximate results with the results obtained with the QMC at $T = 0.5$. In the next subsection we study $\chi(q)$ at low temperatures using the approximation chosen in this subsection.

In Fig. 3.6, results of the uniform susceptibility calculated with the various approximations mentioned in §3.1.3 together with the QMC result, are plotted as

functions of U. All results of the approximate calculations correctly take account of

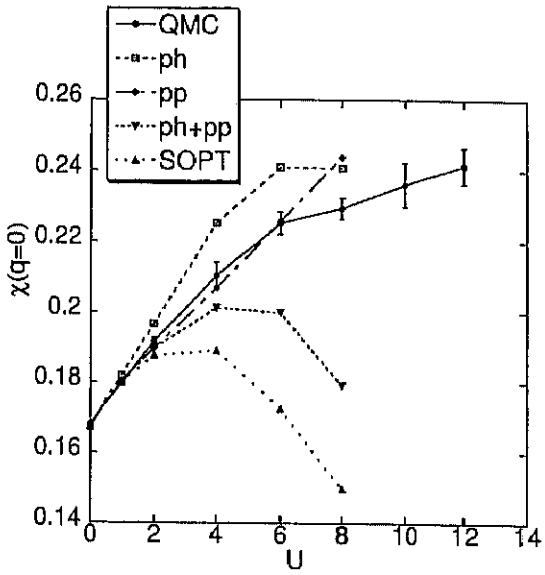

Figure 3.6: Comparison of FLEX, SOPT and QMC results for the uniform susceptibility $\chi(q = 0)$ as functions of U. All results are for $T = 0.5$, $N = 8 \times 8$ and n=0.186.

the contributions of $O(U^2)$. Therefore these results agree with the QMC result as far as U is small, $U \lesssim 1$.

It can be readily seen that $\chi^{(ph)}$ calculated with the FLEX and $\chi^{(pp)}$ calculated with the T-matrix approximation agree well with the exact result obtained with the QMC[1] ; in particular, the T-matrix approximation is found to be accurate as far as the uniform susceptibility is concerned. Furthermore, we examine which one, $\chi^{(ph)}(q)$ or $\chi^{(pp)}(q)$, approximates the wave number dependence of $\chi(q)$ more

[1] The uniform susceptibility obtained with the QMC increases as U gets strong. It can be seen that the second derivative of the uniform susceptibility with respect to U is negative near $U = 0$. (This was also obtained in the previous study [16].) This is why, as seen in Fig. 3.6, the uniform susceptibility $\chi^{(2)}(q)$ obtained with SOPT decreases at $U \gtrsim 4$ and deviates from the exact results for larger U. The SOPT is thus a poor approximation for the large U region where the wave number dependence due to the correlation effect emerges. The uniform susceptibility $\chi^{(ph+pp)}$ obtained by considering the contributions of the particle-hole scattering and of the particle-particle scattering also decreases as U becomes large for large U. Note that although the calculation of $\chi^{(ph+pp)}$ includes more processes than that of $\chi^{(ph)}$ and that of $\chi^{(pp)}$, this approximation is not better than the FLEX and the T-matrix approximation.

closely. We then find that, while $\chi^{(pp)}(q)$ has little dependence on q like $\chi^{(RPA)}(q)$ calculated with the RPA and does not approximate the wave number dependence well, $\chi^{(ph)}(q)$ has a maximum at $q \sim 0$ and is close to the exact results if the strength of interaction U is replaced with a renormalized value $\tilde{U}$, i.e. $\chi^{(ph)}(q;\tilde{U}) \sim \chi(q;U)$ for $U = 12$, $\tilde{U} = 6$ as seen in Fig. 3.7. Moreover, it is found that as temperature is

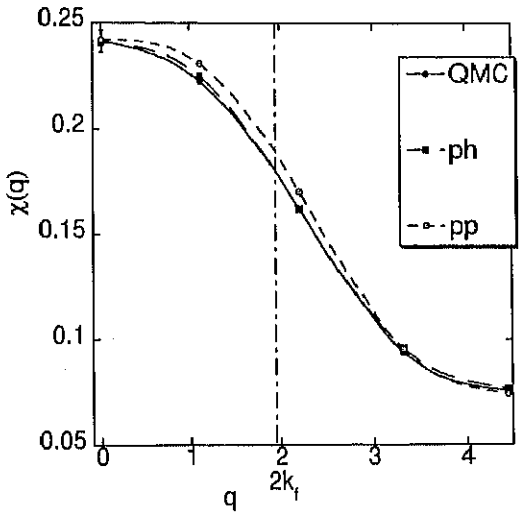

Figure 3.7: Comparison of the static spin susceptibility $\chi(q)$ obtained with the FLEX at $U = 6$, with the T-matrix approximation at $U = 8$ and with the QMC at $U = 12$. The results are for $T = 0.5$, $N = 8 \times 8$ and n=0.186.

lowered, $\chi^{(pp)}(q)$ gets flattened at $q \simeq 0$ as $\chi^{(RPA)}$ does (See Appendix 3.E.). This is in contrast to the exact results. Because of these observations, we use the FLEX to study the wave number dependence of $\chi(q)$ at lower temperatures in the next subsection.

3.2.3 FLEX at low temperatures

In this subsection we show $\chi^{(ph)}(q)$ calculated with the FLEX at low temperatures. The calculation is performed on a lattice with $N = 32 \times 32$.

In Fig. 3.8, we show the static spin susceptibility $\chi(q)$ obtained with the FLEX for different values of U for $T = 0.1$ and $n = 0.1$. Since the fermi energy ε_F for $U = 0$ at $n = 0.1$ is given by $\epsilon_F = 0.5$, $\frac{T}{\varepsilon_f} = 0.2$. It can be seen that a maximum at $q = 0$ develops as the interaction U gets strong.

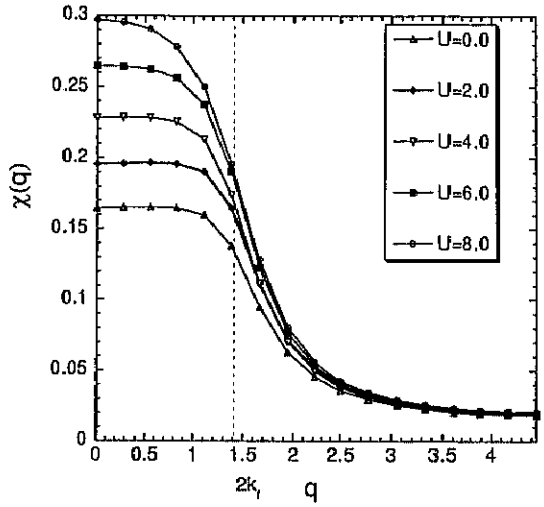

Figure 3.8: The static spin susceptibility $\chi^{(ph)}(q)$ obtained with the FLEX at $T = 0.1$, $N = 32 \times 32$ and $n = 0.1$ for various values of U.

3.2.4 Quasiparticle dispersion

From the previous QMC calculations and FLEX results, it is now almost clear that the ferromagnetic wave number dependence of $\chi(q)$ is developed by the correlation effect as T is lowered. The temperature where the FLEX calculation is performed is still $T = 0.2\varepsilon_F$, which is not very low. One may then object that the ferromagnetic wave number dependence is owing to a finite temperature effect and it will diminish at lower temperatures. Unfortunately, as the calculation including the vertex correction is difficult to perform at lower temperatures, we cannot directly answer this possible objection. We can, however, obtain an inference on the wave number dependence of $\chi(q)$ at lower temperatures by looking into the origin of the wave number dependence.

First, we note that the effect of the vertex correction is negligibly small in the FLEX (i.e. $\chi_0^{(ph)}(q) \simeq \chi^{(ph)}(q)$) as shown in Appendix 3.C. The spin susceptibility $\chi_0(q)$ is given by

$$\chi_0(q) = \frac{2P_0(q)}{1 - UP_0(q)}, \tag{3.35}$$

where $P_0(q)$ is defined by

$$P_0(q) = -\sum_k G(q+k)G(k). \tag{3.36}$$

The wave number dependence is therefore brought about by the selfenergy effect. The calculation of the selfenergy and $\chi_0^{(ph)}(q)$ can be carried out at lower temperatures. In Fig. 3.9, we show $\chi_0^{(ph)}(q)$ at lower temperatures, $T = 0.05 = 0.1\varepsilon_F$, together with $\chi^{(ph)}(q)$ at $T = 0.1 = 0.2\varepsilon_F$. Note that a lattice larger by 16 times

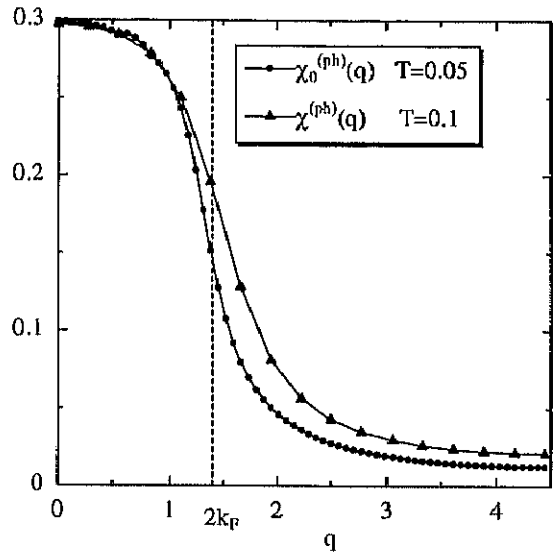

Figure 3.9: The susceptibility $\chi_0^{(ph)}(q)$ obtained with the FLEX at $T = 0.05 = 0.1\varepsilon_F$, $N = 128 \times 128$ and $U = 8.0$, and the susceptibility $\chi^{(ph)}(q)$ obtained with the FLEX at $T = 0.1 = 0.2\varepsilon_F$, $N = 32 \times 32$ and $U = 8.0$.

is needed to go down to a temperature smaller by a factor 2. We can see that the ferromagnetic wave number dependence remains at lower temperatures.

The selfenergy can affect the quasiparticle dispersion through its frequency dependence and its wave number dependence. We show that the wave number dependence of $\chi(q)$ can be mainly accounted for by the wave number dependence of $\Sigma(k)$.

The quasiparticle dispersion E_k is defined by

$$E_k - \xi_k - \tilde{\Sigma}(k, E_k) = 0, \tag{3.37}$$

where we carry out the analytic continuation of the selfenergy from the Matsubara frequency $i\varepsilon_n$ to the real frequency axis Z using the Padé approximation [17], $\Sigma(k, i\varepsilon_n) \to \tilde{\Sigma}(k, Z)$. We denote the susceptibility of free fermions having the dispersion E_k by $\tilde{\chi}(q)$

$$\tilde{\chi}(q) = -2 \int \frac{d^2k}{(2\pi)^2} \frac{f(E_{k-q}) - f(E_k)}{E_{k-q} - E_k}. \tag{3.38}$$

It should be noted that $\tilde{\chi}(q)$ contains no effect of vertex correction; the wave number dependence of the selfenergy is fully considered, but the frequency dependence is only partly considered. The quasiparticle dispersion $E_k^{(ph)}$ obtained with the FLEX at $T = 0.1$, $N = 32 \times 32$ and $U = 8.0$, is shown in Fig. 3.10 together with a parabolic curve. It can readily be seen that $E_k^{(ph)}$ deviates from the parabolic curve and results in ferromagnetic wave number dependence in $\tilde{\chi}^{(ph)}(q)$ as seen in Fig. 3.11. This demonstrates that the deviation of the quasiparticle dispersion E_k from a simple parabola accounts for the ferromagnetic wave number dependence of the susceptibility.

In Fig. 3.12, is shown the dispersion $E_k^{(ph)}$ obtained with the FLEX at $T = 0.05 = 0.1\varepsilon_F$. It is again obvious that $E_k^{(ph)}$ deviates from a parabola. The resultant $\tilde{\chi}^{(ph)}(q)$ is indeed of ferromagnetic wave number dependence (Fig. 3.13). From the calculations of the susceptibility $\chi_0^{(ph)}(q)$ and the quasiparticle dispersion $E_k^{(ph)}$ at lower temperatures, it is clear that the ferromagnetic wave dependence is a genuine feature at $T \to 0$, not a result of a finite temperature effect.

Lastly we also calculate the dispersion $E_k^{(pp)}$ and $\tilde{\chi}^{(pp)}(q)$ using the results of the T-matrix approximation. It is found that $E_k^{(pp)}$ closely follows a parabola (Fig. 3.14) and the resultant $\tilde{\chi}^{(pp)}(q)$ has little wave number dependence (Fig. 3.15) as expected.

3.2.5 Effective interaction

We calculate the effective interaction between quasiparticles mediated by spin fluctuations by using Eqs. (3.32) and (3.33). In the calculation we use the susceptibility obtained with the FLEX at $T = 0.1$ and $n = 0.1$. For comparison, we also calculate the effective interaction using the RPA susceptibility [2] .

[2] If the RPA is used, no effective interaction is generated in channels with finite angular momenta at $T = 0$ because of the independence of the susceptibility on the wave number at $q \leq 2k_F$. At finite

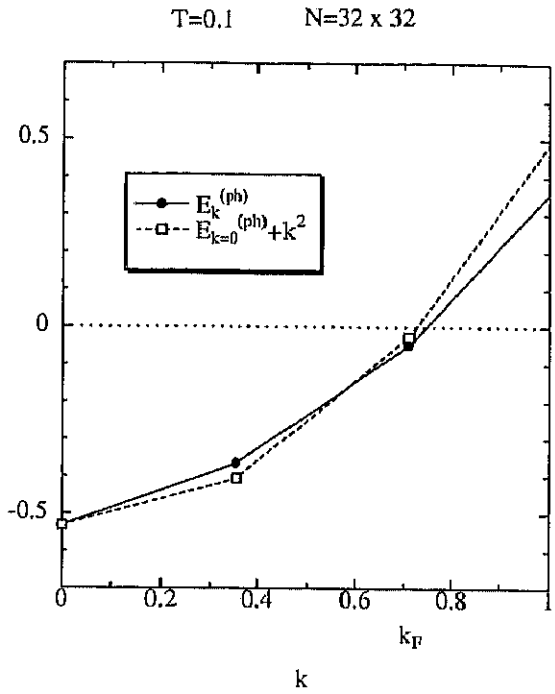

Figure 3.10: The quasiparticle dispersion $E_k^{(ph)}$ obtained with the FLEX at $T = 0.1$, $N = 32 \times 32$ and $U = 8.0$.

We find that the interaction in the s-wave channel is always repulsive and that the most attractive interaction is in the d-wave channel or in the p-wave channel. In Fig. 3.16, we show the ratio of strength of effective interaction in the p-wave channel to that in the d-wave channel as a function of U. For $U \lesssim 5$, the d—wave components is the most attractive both in the RPA and in the FLEX. In the FLEX, however, the p-wave interaction takes the place of the d-wave one to become the most attractive as U gets strong and a maximum of $\chi(q)$ develops at q=0.

It should be noted that an attractive interaction does not necessarily imply an occurrence of the transition to a superfluid state. We have obtained a finite attractive

temperatures, the susceptibility weakly depends on q at $q \lesssim 2k_F$. This lead to a weak attractive interaction in the d-wave channel.

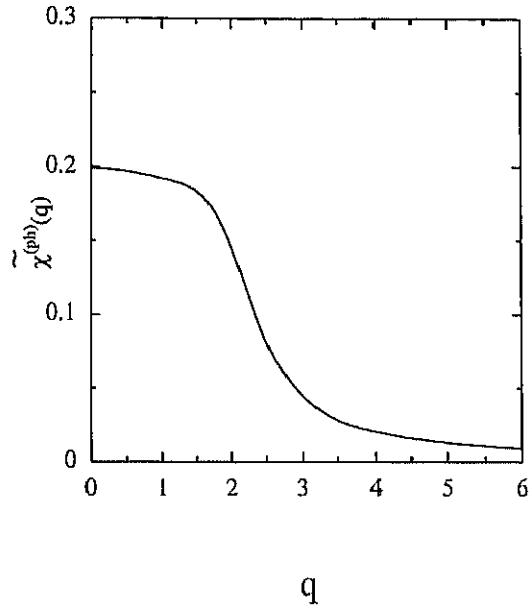

Figure 3.11: The susceptibility $\tilde{\chi}^{(ph)}(q)$ obtained from the quasiparticle dispersion $E_k^{(ph)}$ at $T = 0.1$, $N = 32 \times 32$ and $U = 8.0$.

interaction using the RPA. This is because we have used the susceptibility at a finite temperature ($T = 0.1$). Using this attractive interaction, we would obtain a finite transition temperature, which would be much smaller than $T = 0.1$. At this small temperature, however, the effective interaction calculated with the RPA susceptibility will be much smaller, probably almost vanishing. This means a finite transition temperature obtained with a finite temperature RPA susceptibility is an unreachable possibility. What is important is thus that a finite attractive interaction remains finite as $T \to 0$. From the discussion given in §3.2.4, we can expect that a finite p-wave attractive interaction remains finite and is possibly slightly larger that the one obtained at a finite temperature.

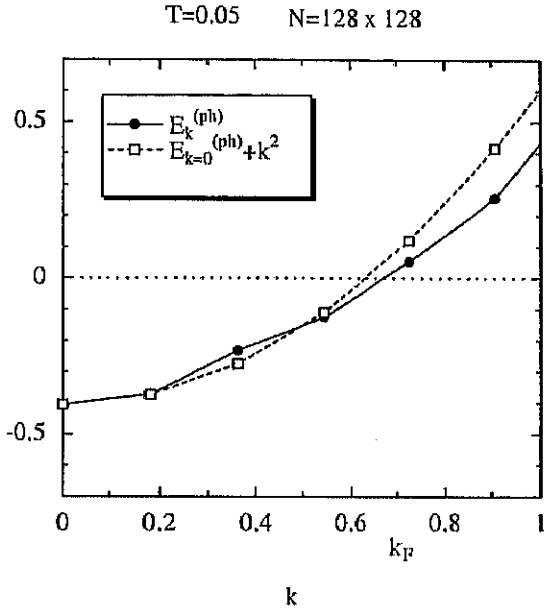

Figure 3.12: The quasiparticle dispersion $E_k^{(ph)}$ obtained with the FLEX at $T = 0.05$, $N = 128 \times 128$ and $U = 8.0$.

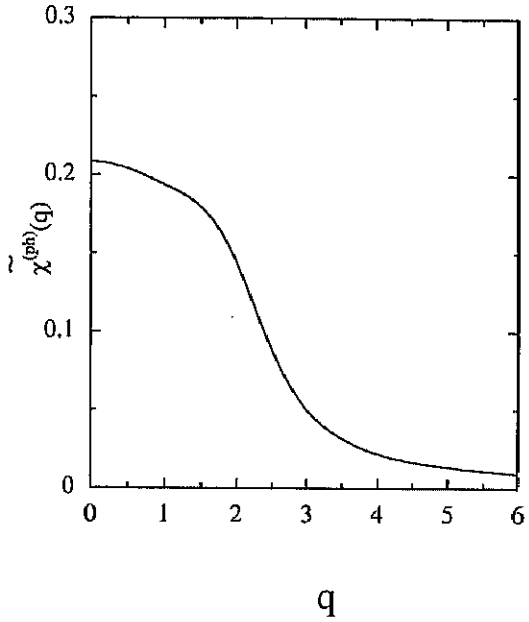

Figure 3.13: The susceptibility $\tilde{\chi}^{(ph)}(q)$ obtained from the quasiparticle dispersion $E_k^{(ph)}$ at $T = 0.05$, $N = 128 \times 128$ and $U = 8.0$.

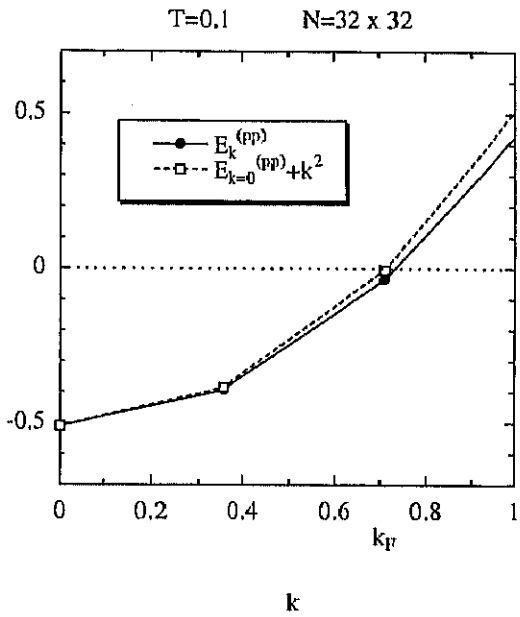

Figure 3.14: The quasiparticle dispersion $E_k^{(pp)}$ obtained with the T-matrix approximation at $T = 0.1$, $N = 32 \times 32$ and $U = 8.0$.

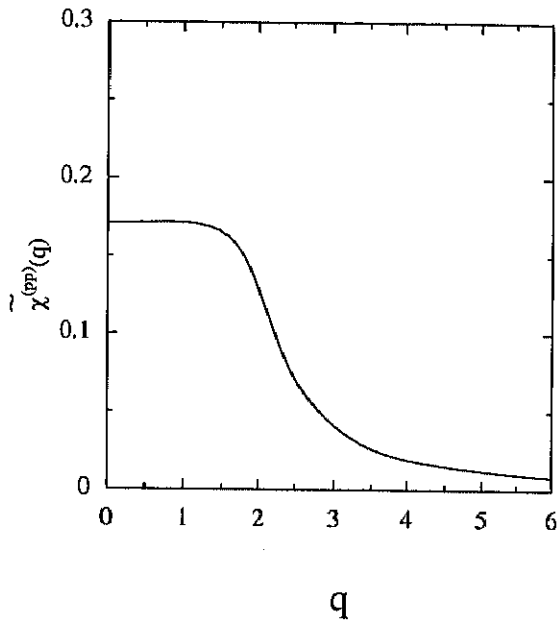

Figure 3.15: The susceptibility $\tilde{\chi}^{(pp)}(q)$ obtained from the quasiparticle dispersion $E_k^{(pp)}$ at $T = 0.1$, $N = 32 \times 32$ and $U = 8.0$.

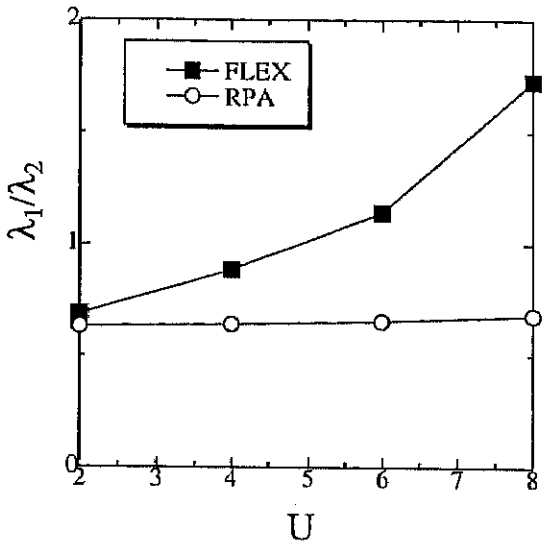

Figure 3.16: The ratio of strength of effective interaction λ_1 in the p-wave channel to that λ_2 in d-wave channel as a function of U

3.3 Summary and discussion

In this chapter we have studied the static spin susceptibility $\chi(q)$ and the effective interaction between quasiparticles in the dilute two-dimensional Hubbard model by applying the quantum Monte Carlo method (QMC) and the fluctuation exchange approximation (FLEX). The principal results to be drawn from this study are as follows:

1. The FLEX is a good approximation in calculating the wave number dependence of the static spin susceptibility (at least where the reliable results are obtained by the QMC).

2. A maximum at wave number $q = 0$ emerges and develops in $\chi(q)$ as the interaction U gets strong.

3. A maximum at $q = 0$ emerges and develops in $\chi(q)$ as temperature is lowered.

4. The most attractive component of the effective interaction mediated by spin fluctuations is the p-wave component in the strong coupling region where a maximum at $q = 0$ develops in $\chi(q)$.

Baranov, Kagan and Chubukov [18, 19, 20] once studied the Cooper instability in the dilute 2D Hubbard model on the square lattice. They calculated the effective interaction in the Cooper channel with the second order perturbation theory. They expanded the spectrum on the square lattice, $\xi_k = -2t(\cos k_x + \cos k_y)$, till higher order terms. Expanding the spectrum ξ_k till the sixth order terms, $\xi_k = \frac{k^2}{2m_3} - \frac{1}{24m_3}(k_x^2 + k_y^2) - \frac{1}{720m_3}(k_x^6 + k_y^6) - \mu$, they found attractive interaction was generated in the d-wave channel. They further studied the Cooper instability taking account of diagrams beyond the second order diagrams and found that the p-wave pairing occurred in the strong coupling region. These results agree with ours in that the p-wave pairing arises only when higher order diagrams are included in the effective interaction.

Ohnishi and Miyake [21] also studied the Cooper instability using paramagnon theory in short-ranged interacting 2D fermion systems. They used the RPA susceptibility, but took account of frequency dependence and momentum dependence of interaction more seriously.(They considered retardation effect and also removed the restriction that the interacting particles were just on the fermi line.) They then found that the d-wave interaction was the most dominant. Certainly the frequency dependence of the effective interaction can be essentially important in discussing the pairing instability. At the same time, strong correlation effect is equally important in liquid ^{3}He. It is possible that the interaction in the p-wave channel dominates over that in the d-wave one in the strong coupling region even when frequency dependence is fully considered. Study taking account of both strong correlation effect and frequency dependence of interaction is an important subject of a future study.

The model and results obtained here are directly applied to dilute ^{3}He films where the radius of the hard core is much smaller than the inter-particle distance. For dense 2D liquid ^{3}He, use of a lattice model becomes questionable. Moreover, at high densities, the momentum dependence of the interaction potential should be seriously considered in the calculations of susceptibility. For dense 2D ^{3}He, a microscopic theory which starts from a realistic potential such as the Lennard-Jones potential is necessary, which is also a subject of future study.

Appendix

3.A The quantum Monte Carlo method in the 2D Hubbard model

The approach for simulating the grand canonical ensemble in the 2D Hubbard Model was formulated by several authors [7, 10]. In this section, we outline the algorithm of the grand canonical quantum Monte Carlo method in the 2D Hubbard model. The expectation value of a physical observable, O, is given by

$$< O >= \frac{Tr\, O e^{-\beta \mathcal{H}}}{Tr\, e^{-\beta \mathcal{H}}}, \tag{3.39}$$

where β is the inverse temperature, and $\mathcal{H}$ is the Hamiltonian. The 2D Hubbard model has the following form in real space,

$$\mathcal{H} = \mathcal{H}_K + \mathcal{H}_U, \tag{3.40}$$

where

$$\mathcal{H}_K = -t \sum_{<i,j>,\sigma} (a^\dagger_{i\sigma} a_{j\sigma} + a^\dagger_{j\sigma} a_{i\sigma}) - \bar{\mu} \sum_{i=1}^{N} (n_{i\uparrow} + n_{i\downarrow}) \equiv \sum_{<i,j>,\sigma} a^\dagger_{i\sigma} K_{ij} a_{j\sigma}, \tag{3.41}$$

and

$$\mathcal{H}_U = U \sum_{i=1}^{N} (n_{i\uparrow} - \frac{1}{2})(n_{i\downarrow} - \frac{1}{2}). \tag{3.42}$$

Here $a_{i\sigma}(a^\dagger_{i\sigma})$ is the annihilation(creation) operator for fermions of spin σ at site i, $n_{i\sigma} = a^\dagger_{i\sigma} a_{i\sigma}$, t is the hopping parameter, U is the on-site repulsion, $\bar{\mu}$ is the chemical potential, and N is the total number of the lattice points. The sum $< i, j >$ is over the all pairs of the nearest neighbor sites.

In order to perform numerical simulations, we first carry out the traces over the fermion degrees of freedom. By Suzuki-Trotter break up, the partition function of the system is approximated for large $L \gg 1$ (L is the Trotter number) as follows,

$$Z \equiv Tr\, e^{-\beta \mathcal{H}} = Tr \prod_{\ell=1}^{L} e^{\Delta\tau \mathcal{H}} \simeq Tr \prod_{\ell=1}^{L} e^{\Delta\tau \mathcal{H}_U} e^{\Delta\tau \mathcal{H}_K}, \tag{3.43}$$

where $\Delta\tau = \frac{\beta}{L}$. Errors resulting from finiteness of $\Delta\tau$ is known to be of the order of $(\Delta\tau)^2$. The interaction terms, $\exp(-\Delta\tau \mathcal{H}_U)$, can be made quadratic in the fermion

creation and annihilation operators by introducing a discrete Hubbard-Stratonovich transformation

$$e^{-\Delta\tau U(n_{i\uparrow}-\frac{1}{2})(n_{i\downarrow}-\frac{1}{2})} = \frac{1}{2}e^{\frac{-\Delta\tau U}{4}} \sum_{\{s_{i,l}=\pm 1\}} e^{-\Delta\tau s_{i,l}\alpha(n_{i\uparrow}-n_{i\downarrow})}, \tag{3.44}$$

at each lattice point i and at each imaginary time slice l. α is defined by the relation $\cosh(\Delta\tau\alpha) = e^{(\frac{\Delta\tau U}{2})}$. The transformation reduces the problem to that of non-interacting fermions in a time-dependent Hubbard-Stratonovich spin field $s_{i,l}$. As a result, the trace over the fermion degrees of freedom can be preformed and the partition function is given by

$$Z = \sum_{\{s_{i,l}=\pm 1\}} \det M^{\uparrow} \det M^{\downarrow}, \tag{3.45}$$

with

$$M^{\sigma} = I + B^{\sigma}_{L} B^{\sigma}_{L-1} \cdots B^{\sigma}_{1}, \tag{3.46}$$

and

$$B^{\sigma}_{l} = \exp(-(\mathrm{sgn}\sigma)\Delta\tau \boldsymbol{S}(l)) \exp(-\Delta\tau K). \tag{3.47}$$

$\boldsymbol{I}$ is the $N \times N$ unit matrix and $S_{ij}(l) = \delta_{ij} s_{i,l}$. Then Eq. (3.39) can be written by

$$< O >= \sum_{\{s_{i,l}=\pm\}} < O >_{s} P(\{s_{i,l}\}), \tag{3.48}$$

where $< O >_{s}$ is the expectation value for a fixed set of fields $\{s_{i,l}\}$ and the probability distribution $P(\{s_{i,l}\})$ is given by

$$P(\{s_{i,l}\}) = \frac{\det M^{\uparrow} \det M^{\downarrow}}{Z}. \tag{3.49}$$

Since $< O >_{s}$ is an average for particles which interacts only with auxiliary fields $\{s_{i,l}\}$ and not with each other, we can apply Wick's theorem to it and $< O >_{s}$ can be expressed in terms of the Green's function.

Once the trace over the fermion degrees of freedom has been performed, we can use standard Monte Carlo techniques to evaluate the right-hand side of Eq. (3.48). We wish to obtain a sequence of spin configurations, $\{s_{i,l}\}$, with the probability distribution $P(\{s_{i,l}\})$. Now in order to update the spin variable $s_{i,l}$ using any standard algorithm, such as heat bath or Metropolis, we must calculate the change in the probability distribution $P(\{s_{i,l}\})$ when $s_{i,l} \rightarrow -s_{i,l}$. Under this change,

$$\boldsymbol{A}^{\sigma}(l) \rightarrow \boldsymbol{A}^{\sigma}(l)' = [\boldsymbol{I} + \boldsymbol{\Delta}^{\sigma}(i,l)]\boldsymbol{A}^{\sigma}(l), \tag{3.50}$$

where $\boldsymbol{A}^{\sigma}(l)$ is defined by

$$\boldsymbol{A}^{\sigma}(l) = B_l^{\sigma} \cdots \boldsymbol{B}_1^{\sigma} \boldsymbol{B}_L^{\sigma} \cdots \boldsymbol{B}_{l+1}^{\sigma}, \tag{3.51}$$

and $\boldsymbol{\Delta}^{\sigma}(i,l)$ is a matrix with only one nonzero element,

$$\Delta^{\sigma}(i,l)_{jk} = \delta_{ji}\delta_{ki}(e^{(\mathrm{sgn}\sigma)2\Delta\tau\alpha s_{i,l}} - 1). \tag{3.52}$$

The ratio of the probability distribution $P(\{s_{i,l}\})$ after and before the spin flip is given by

$$R = R^{\uparrow}R^{\downarrow}, \tag{3.53}$$

where

$$R^{\sigma} = \frac{\det M^{\sigma\prime}}{\det M^{\sigma}} = \det[\boldsymbol{I} + \boldsymbol{G}^{\sigma}(l)\boldsymbol{\Delta}^{\sigma}(i,l)\boldsymbol{A}^{\sigma}(l)] = 1 + [1 - G^{\sigma}(l)_{ii}]\Delta^{\sigma}(i,l)_{ii}. \tag{3.54}$$

Here $\boldsymbol{G}^{\sigma}(l)$ is the equal-time Green's function for a fermion propagating through the field produced by the $s_{i,l}$,

$$G^{\sigma}(l)_{ij} = < T_{\tau}[a_{i\sigma}(l\Delta\tau)a_{j\sigma}^{\dagger}(l\Delta\tau)] >= [I + A^{\sigma}(l)]_{ij}^{-1}. \tag{3.55}$$

The rate of the probability distribution $P(\{s_{i,l}\})$ is expressed by only the Green's function, which is one of the most remarkable features of the algorithm. Thus we can obtain $< O >$ if we can calculate the Green's function at an individual Monte Carlo step.

We have now assembled all of the ingredients necessary to carry out simulations. However, actually there are some problems to perform simulations at low temperatures. At low temperatures, the grand canonical QMC algorithm becomes increasingly useless not only because the numerical effort to go to lower temperatures itself increases the computer time, but also because numerical instabilities start to dominate at low temperatures. To perform simulations, we must compute the Green's function , i.e., the matrices $\boldsymbol{A}^{\sigma}(l)$, to sufficient accuracy. This becomes increasingly difficult as the temperature is lowered. For example, for the 2D Hubbard Model with $U = 0$, the $\boldsymbol{A}^{\sigma}(l)$ have eigenvalues as large as $\exp(4t\beta)$ and as small as $\exp(-4t\beta)$. If we calculated $\boldsymbol{A}^{\sigma}(l)$ simply by multiplying $\boldsymbol{B}_m^{\sigma}$ iteratively in Eq. (3.51), therefore, round-off errors would dominate and no reliable results could be obtained at low temperatures such as at $\beta = 2/t$, where we carry out the calculation. To avoid this difficulty, we have to separate the contribution from the large eigenvalues and that from the small eigenvalues and perform the multiplication in Eq. (3.51) carefully.

This problem can indeed be dealt with a relatively straightforward manner using matrix factorization methods [7, 10]. Suppose that one can multiply m of the $\boldsymbol{B}_l^{\sigma}$

without losing numerical accuracy. We then use the Gram-Schmidt orthogonalization procedure to write this product in the form

$$a_1^\sigma(l) = B_{l+m}^\sigma B_{l+m-1}^\sigma \cdots B_{l+1}^\sigma = U_1^\sigma D_1^\sigma R_1^\sigma, \tag{3.56}$$

where U_1^σ is an orthogonal matrix, D_1^σ a diagonal matrix, and R_1^σ a right triangular matrix with diagonal elements equal to one. The orthogonal matrix U_1^σ is necessarily well conditioned and R_1^σ need not be well conditioned, but in practice it is. Only the diagonal matrix D_1^σ has large variations in the size of its elements. We next form

$$a_2^\sigma(l) = B_{l+2m}^\sigma \cdots B_{l+1}^\sigma = B_{l+2m}^\sigma \cdots B_{l+m+1}^\sigma U_1^\sigma D_1^\sigma R_1^\sigma, = U_2^\sigma D_2^\sigma R_2^\sigma. \tag{3.57}$$

The order of operations in Eq. (3.57) is important. We first multiply U_1^σ by $B_{l+2m}^\sigma \cdots B_{l+m+1}^\sigma$. By assumption, m is small enough so that this matrix can be computed accurately. We then multiply it on the right by D_1^σ. This only rescales the columns of the matrix, and thus does no harm to the numerical stability of the next step, a UDR decomposition of this partial product. We then multiply the resulting triangular matrix on the right by R_1^σ to obtain the last line of Eq. (3.57). This process is repeated $\frac{L}{m}$ times to obtain,

$$A^\sigma(l) = a_{\frac{L}{m}}^\sigma(l) = U_{\frac{L}{m}}^\sigma D_{\frac{L}{m}}^\sigma R_{\frac{L}{m}}^\sigma. \tag{3.58}$$

Thus these numerical instabilities are suppressed by the UDR decomposition scheme. For the present simulations where a temperature is lowered down to $\frac{t}{2}$, we can remove the numerical instabilities efficiently by the UDR decomposition scheme.

Another possible obstacle to go down to low temperatures is the "negative sign" problem. So far we have implicitly assumed that $P(\{s_{i,l}\})$ is positive semidefinite so that it can be regarded as a probability distribution function. Unfortunately, this is not always the case for fermion problems because of the anticommuting nature of fermions. In cases where the probability distribution $P(\{s_{i,l}\})$ is not positive semidefinite, one uses $|P(\{s_{i,l}\})|$ as the probability distribution, and the expectation value of an observable O is calculated as

$$< O >_P = \frac{< O \mathrm{sgn} P >_{|P|}}{< \mathrm{sgn} P >_{|P|}}, \tag{3.59}$$

where the subscript P and $|P|$ indicate averages taken with the distributions $P(\{s_{i,l}\})$ and $|P(\{s_{i,l}\})|$, respectively. However, if the average sign, $< \mathrm{sgn} P >_{|P|}$, is close to zero, this estimator for $< O >_P$ is very noisy. Generally the "negative sign" problem is very serious for simulations of fermions at low temperatures because no useful

means to overcome it is discovered. In the dilute limit, the "negative sign" problem is not so serious. Actually, in the present study, we do not go down to the low-temperature regime where the "negative sign" problem becomes serious, because finite size effects become too large for the results to be reliable before the "negative sign" problem gets serious. In the present simulations, the probability distribution is almost positive-semidefinite.

3.B Aslamasov-Larkin diagrams in the irreducible four-point vertex function

We neglect contributions of Aslamasov-Larkin (AL) diagrams and consider only contributions of Maki-Thompson diagrams (MT) in the irreducible four-point vertex function because of difficulty of calculations. While there is one spin fluctuation propagator in MT diagrams, there are two spin fluctuation propagators in AL diagrams. Therefore, at first sight, it appears that contribution of AL diagrams is greater than that of MT diagrams when spin fluctuations are strongly enhanced and that an approximation omitting AL diagrams is a poor one. In this section, it is argued that contribution of AL diagrams is at most of the same order as contribution of MT diagrams when spin fluctuations are strongly enhanced [22].

In the FLEX, there are six kinds of AL diagrams:

$$\begin{aligned}\gamma_{-}^{(AL)}(q;k,k') = & \\ & \gamma_{\uparrow\uparrow\uparrow\uparrow}^{(AL,a)}(q;k,k') + \gamma_{\uparrow\uparrow\uparrow\uparrow}^{(AL,b)}(q;k,k') + \gamma_{\uparrow\uparrow\uparrow\uparrow}^{(AL,c)}(q;k,k') \\ & -\gamma_{\uparrow\downarrow\downarrow\uparrow}^{(AL,d)}(q;k,k') - \gamma_{\uparrow\downarrow\downarrow\uparrow}^{(AL,e)}(q;k,k') \\ & -\gamma_{\uparrow\downarrow\downarrow\uparrow}^{(AL,f)}(q;k,k'), \end{aligned} \tag{3.60}$$

Each contribution is expressed as (See Figs. 3.17(a)- Fig. 3.17(f).)

$$\begin{aligned}\gamma_{\uparrow\uparrow\uparrow\uparrow}^{(AL,a)}(q;k,k') = & \sum_{k''} G(k'')U^2\pi_o(k+q-k'') \\ & \times U^2\pi_o(k''-k)G(k'+k''-k), \end{aligned} \tag{3.61}$$

$$\begin{aligned}\gamma_{\uparrow\uparrow\uparrow\uparrow}^{(AL,b)}(q;k,k') = & \sum_{k''} G(k''+q)U^2\pi_o(k-k'') \\ & \times U^2\pi_o(k''+q-k)G(k+k'-k''), \end{aligned} \tag{3.62}$$

$$\gamma_{\uparrow\uparrow\uparrow\uparrow}^{(AL,c)}(q;k,k') =$$

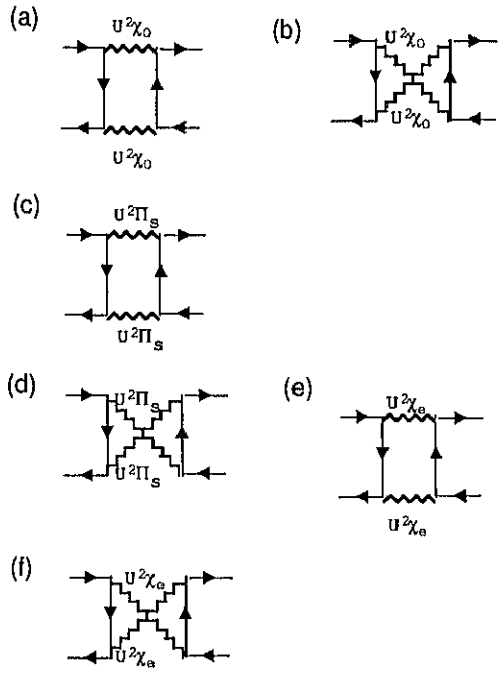

Figure 3.17: Diagrams representing AL diagrams. The wavy line represents $U^2\pi_o$, $U^2\pi_e$ or $U^2\Pi_s$. (a) $\gamma^{(AL,a)}_{\uparrow\uparrow\uparrow\uparrow}(q;k,k'')$, (b) $\gamma^{(AL,b)}_{\uparrow\uparrow\uparrow\uparrow}(q;k,k'')$, (c) $\gamma^{(AL,c)}_{\uparrow\uparrow\uparrow\uparrow}(q;k,k'')$, (d) $\gamma^{(AL,d)}_{\uparrow\downarrow\downarrow\uparrow}(q;k,k'')$, (e) $\gamma^{(AL,e)}_{\uparrow\downarrow\downarrow\uparrow}(q;k,k'')$, and (f) $\gamma^{(AL,f)}_{\uparrow\downarrow\downarrow\uparrow}(q;k,k'')$.

$$\times U^2 \sum_{k'} G(k'')\{[1+U\Pi_s(k+q-k'')]$$
$$\times[1+U\Pi_s(k''-k)]-1\}G(k'+k''-k), \tag{3.63}$$

$$\gamma^{(AL,d)}_{\uparrow\downarrow\downarrow\uparrow}(q;k,k') =$$
$$\times U^2 \sum_{k''} G(k''+q)\{[1+U\Pi_s(k-k'')]$$
$$\times[1+U\Pi_s(k''+q-k)]-1\}G(k+k'-k''), \tag{3.64}$$

$$\gamma^{(AL,e)}_{\uparrow\downarrow\downarrow\uparrow}(q;k,k') =$$
$$\times U^2 \sum_{k''} G(k'')\{[1+U\pi_e(k+q-k'')]$$
$$\times[1+U\pi_e(k''-k)]-1\}G(k'+k''-k), \tag{3.65}$$

$$\gamma^{(AL,f)}_{\uparrow\downarrow\downarrow\uparrow}(q;k,k') =$$
$$\times U^2 \sum_{k''} G(k''+q)\{[1+U\pi_e(k-k'')]$$
$$\times[1+U\pi_e(k''+q-k)]-1\}G(k+k'-k''), \tag{3.66}$$

where $\pi_o(q)$ and $\pi_e(q)$ is defined as

$$\pi_o(q) = \frac{1}{2}(\Pi_c(q)+\Pi_s(q)), \tag{3.67}$$

and

$$\pi_e(q) = -\frac{1}{2}(\Pi_c(q)-\Pi_s(q)). \tag{3.68}$$

If spin fluctuations are strongly enhanced, π_o and π_e can be approximated as

$$\pi_o(q) \sim \frac{1}{2}\Pi_s(q), \tag{3.69}$$

and

$$\pi_e(q) \sim \frac{1}{2}\Pi_s(q). \tag{3.70}$$

Furthermore, if ferromagnetic spin fluctuations are strongly enhanced, $\Pi_s(q)$ has a strong maximum Π_s^* at $q=(q=0,\omega_n=0)$ and $\Pi_s(q)$ in Eq. (3.61)-(3.66) can be approximated as

$$\Pi_s(q) = \Pi_s^* \delta_{q,0}\delta_{\omega_n,0}. \tag{3.71}$$

Each term, Eq. (A.i) (i=2,...,7), is of $O(\Pi_s^{*2})$ while contribution of MK diagrams is of $O(\Pi_s^*)$. However it can be readily confirmed that the leading terms cancel each other and that contribution of AL diagrams turns out to be of the same order as that of MK diagrams.

3.C Effect of the vertex corrections

We give brief comments on the effect of the vertex corrections in this section. When the vertex corrections are neglected, i.e. $K_{-}(q;k)=1$, the spin susceptibility $\chi_0(q)$ is given by

$$\chi_0(q)=\frac{2P_0(q)}{1-UP_0(q)}, \tag{3.72}$$

where $P_0(q)$ is defined by

$$P_0(q)=-\sum_k G(q+k)G(k). \tag{3.73}$$

As seen in Fig. 3.18, we find that the effect of the vertex corrections of MT (Maki-Thompson) type is negligible in the FLEX, i.e. $\chi_0^{(ph)}(q)\simeq\chi^{(ph)}(q)$. The wave number dependence of $\chi^{(ph)}(q)$ is caused by the effect of selfenergy $\Sigma^{(ph)}$.

On the other hand, in the T-matrix approximation, the effect of the vertex corrections of MT type is quite large. As seen in Fig. 3.19, without taking account of the vertex corrections, one would considerably overestimate the susceptibility. Only with vertex corrections, one can obtain reasonable results for the susceptibility with the T-matrix approximation.

3.D Effective interaction mediated by spin fluctuations and charge fluctuations

We give the expression of effective interaction mediated by spin fluctuations and charge fluctuations in this section. In the static limit, $\tilde{\Gamma}_{\sigma_1\sigma_2\sigma_3\sigma_4}(q;k,k')=\tilde{\Gamma}_{\sigma_1\sigma_2\sigma_3\sigma_4}(q,\mathrm{i}\omega_n;k,\mathrm{i}\varepsilon_m,k'',\mathrm{i}\varepsilon''_m)\longrightarrow\tilde{\Gamma}_{\sigma_1\sigma_2\sigma_3\sigma_4}(q;k,k')$, the effective interaction $\hat{V}$ mediated by spin fluctuations and charge fluctuations can be written as second-quantized form

$$\begin{aligned}\hat{V}=&\frac{1}{2}\sum_{k,k',q}\sum_{\sigma_i}\tilde{\Gamma}_{\sigma_1\sigma_2\sigma_3\sigma_4}(q;k,k')\\&\times\sum_{\sigma\sigma'}a^{\dagger}_{k'}+q,_{\sigma_2}a^{\dagger}_{k,\sigma_4}a_k+q,_{\sigma_1}a_{k',\sigma_3}\end{aligned} \tag{3.74}$$

where $\tilde{\Gamma}_{\sigma_1\sigma_2\sigma_3\sigma_4}$ is a four-point vertex function which represents spin fluctuations and charge fluctuations. In this section, the function $\tilde{\Gamma}_{\sigma_1\sigma_2\sigma_3\sigma_4}$ and $\Gamma_{\sigma_1\sigma_2\sigma_3\sigma_4}$ are defined as the four-point vertex function which represents spin fluctuations and charge fluctuation. A difference between $\tilde{\Gamma}_{\sigma_1\sigma_2\sigma_3\sigma_4}$ and $\Gamma_{\sigma_1\sigma_2\sigma_3\sigma_4}$ is that while $\tilde{\Gamma}_{\sigma_1\sigma_2\sigma_3\sigma_4}$ includes

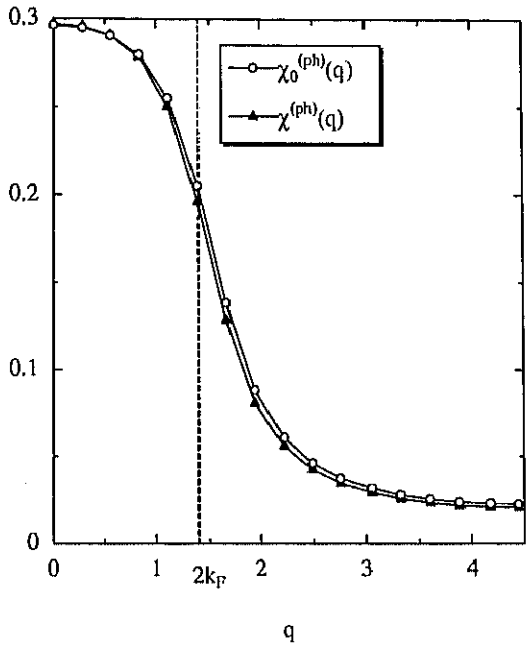

Figure 3.18: The susceptibility $\chi_0^{(ph)}(q)$ and $\chi^{(ph)}(q)$ obtained with the FLEX at $U = 8$, $T = 0.1$, $N = 32 \times 32$ and $n = 0.1$.

diagrams which split into two distinct diagrams when one interaction line is cut, $\Gamma_{\sigma_1\sigma_2\sigma_3\sigma_4}$ do not include those diagrams. It is convenient to separate $\hat{V}$ into two terms, referring to the triplet channel and the singlet channel

$$\begin{aligned}\hat{V} = & \frac{1}{2}\sum_{k,\,k',\,q} V_t(q;k,k') \\ & \times \sum_{\sigma,\sigma'} a^\dagger_{k'+q,\sigma} a^\dagger_{k,\sigma'} a_{k+q,\sigma'} a_{k',\sigma} \\ & + \frac{1}{2}\sum_{k,\,k',\,q} V_s(q;k,k') \\ & \times \sum_{\sigma} a^\dagger_{k'+q,\sigma} a^\dagger_{k,-\sigma} a_{k+q,-\sigma} a_{k',\sigma}\end{aligned} \tag{3.75}$$

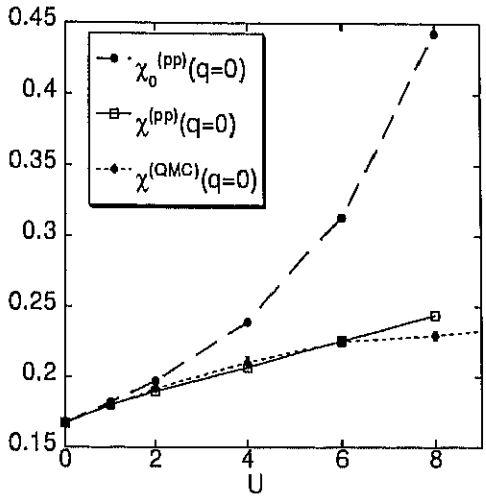

Figure 3.19: $\chi_0^{(pp)}(q=0)$, $\chi^{(pp)}(q=0)$ and $\chi^{(QMC)}(q=0)$ are plotted as functions of U. All results are for $T=0.5$, $N=8\times 8$ and n=0.186.

where

$$
\begin{aligned}
& V_t(q;k,k') \\
&= \frac{1}{4}\left(\tilde{\Gamma}_+(q;k,k') - \tilde{\Gamma}_+(k'-k;k,k+q)\right) \\
&+ \frac{1}{4}\left(\tilde{\Gamma}_-(q;k,k') - \tilde{\Gamma}_-(k'-k;k,k+q)\right), \qquad (3.76)
\end{aligned}
$$

$$
\begin{aligned}
& V_s(q;k,k') \\
&= \frac{1}{4}\left(\tilde{\Gamma}_+(q;k,k') + \tilde{\Gamma}_+(k'-k;k,k+q)\right) \\
&- \frac{3}{4}\left(\tilde{\Gamma}_-(q;k,k') + \tilde{\Gamma}_-(k'-k;k,k+q)\right), \qquad (3.77)
\end{aligned}
$$

(the subscript $\pm$ indicates $O_\pm = O_{\uparrow\uparrow\uparrow\uparrow} \pm O_{\uparrow\downarrow\downarrow\uparrow}$). In Eq. (3.74) and Eq. (3.75), the wave function renormalization z_k is neglected for simplicity, $z_k = 1$. Although z_k is important for determining the transition temperature, z_k can be neglected in discussing the relative intensity of the effective interaction in the d-wave channel to that in the p-wave channel owing to the isotropy of system, $z_k = z_{|k|}$.

The four-point vertex function $\tilde{\Gamma}_\pm(q,k,k')$ satisfies the following relation:

$$
\tilde{\Gamma}_\pm(q;k,k') = \Gamma_\pm(q;k,k') + K_\pm(q;k\,)J^\pm(q)K_\pm(q;k\,), \qquad (3.78)
$$

where $K_{\pm}(q;k)$ is the three-point vertex function which is defined in §3.1 and $J^{\pm}(q)$ is defined as

$$J^{\pm}(q) = \pm\frac{U}{1 \pm UP_{\pm}(q)}. \tag{3.79}$$

When spin fluctuations are much greater than charge fluctuations, i.e. $|\tilde{\Gamma}_{+}| \ll |\tilde{\Gamma}_{-}|$, $\tilde{\Gamma}_{+}$ can be neglected. Furthermore, since the main factor of the enhancement of spin fluctuations is a small denominator $(1-UP_{-}(q))$ in Eq. (3.79), $|\Gamma_{-}|$ is much smaller than the second term. $\tilde{\Gamma}_{-}(q)$can thus be approximated as

$$\tilde{\Gamma}_{-}(q;k,k') \simeq K_{-}(q;k)J^{-}(q)K_{-}(q;k') \tag{3.80}$$

Then the effective interaction $v_t(k,k')$ in the triplet channel is given by

$$\begin{aligned} v_t(k,k') &= \frac{1}{4}\left[\tilde{\Gamma}_{-}(k-k';k,k') - \tilde{\Gamma}_{-}(k+k';k,k')\right] \\ &= \frac{1}{4}\left[K^{*}_{-}(k,k')J^{-}(k-k')K^{*}_{-}(k,k')\right. \\ &- \left. K^{*}_{-}(k',k)J^{-}(k+k')K^{*}_{-}(-k',-k)\right], \end{aligned} \tag{3.81}$$

where $K^{*}_{-}(k,k') = K_{-}(k-k';k')$. Similarly, the effective interaction $v_s(k,k')$ in the singlet channel is given by

$$\begin{aligned} v_s(k,k') &= -\frac{3}{4}\left[\tilde{\Gamma}_{s}(k-k';k,k') + \tilde{\Gamma}_{s}(k+k';k',k)\right] \\ &= -\frac{3}{4}\left[K^{*}_{-}(k,k')J^{-}(k-k')K^{*}_{-}(k,k')\right] \\ &+ \left. K^{*}_{-}(k',k)J^{-}(k+k')K^{*}_{-}(-k',-k)\right]. \end{aligned} \tag{3.82}$$

$K^{*}_{-}(k,k')$ represents "vertex corrections" [23]. Migdal once showed that "vertex corrections" in the electron-phonon interaction could be neglected [23], i.e. $|K^{*}_{-} - 1| = O(\sqrt{m_e/M_{ion}}) \ll 1$ (m_e is mass of electron and M_{ion} is mass of ion). However, it is not obvious that "vertex correction" in the interaction mediated by spin fluctuations can be neglected. In this study, We simply put $K^{*}_{-} = 1$ expecting that the wave number dependence of the interaction, which is the key element to determining the relative intensity of interaction in channels with different angular momenta, is mainly determined by the wave number dependence of $J(q)$. The final expression of the effective interaction in the triplet channel and in the singlet channel are then given by

$$\begin{aligned} v_t(k,k') &= \frac{1}{4}\left[J^{-}(k-k') - J^{-}(k+k')\right] \\ &= -\frac{U^2}{8}\left[\chi(k-k') - \chi(k+k')\right], \end{aligned} \tag{3.83}$$

$$v_s(k,k') = -\frac{3}{4}\left[J^-(k-k') + J^-(k+k')\right]$$
$$= \frac{3U}{2} + \frac{3U^2}{8}[\chi(k-k') + \chi(k+k')]. \quad (3.84)$$

3.E $\chi(q)$ Obtained with T-matrix approximation at low temperatures

In Fig.3.20, we show the static spin susceptibility $\chi^{(pp)}(q)$ for different values of U for $T = 0.1$ and $n = 0.1$. $\chi^{(pp)}(q)$ has little dependence on q at $q \lesssim 2k_F$ like $\chi^{(RPA)}(q)$ obtained with the RPA. $\chi^{(pp)}(q)$ is close to $\chi^{(RPA)}(q)$ if the strength of interaction U is replaced with a renormalized value U^*, i.e. $\chi^{(pp)}(q;U^*) \sim \chi^{(RPA)}(q;U)$ for $U = 14$, $U^* = 3.7$ as seen in Fig. 3.21.

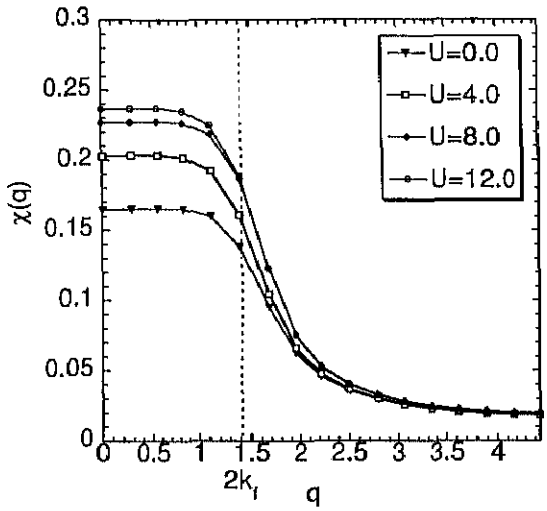

Figure 3.20: The static spin susceptibility $\chi^{(pp)}(q)$ obtained with the $T-$matrix approximation at $T = 0.1$, $N = 32 \times 32$ and $n = 0.1$ for various values of U.

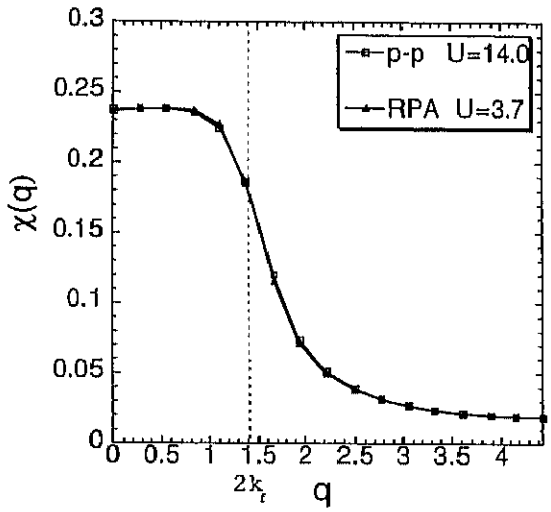

Figure 3.21: Comparison of the static spin susceptibility $\chi^{(pp)}(q)$ obtained with the $T-$matrix approximation at $U = 14$ and $\chi^{(RPA)}(q)$ with the RPA at $U = 3.7$. The results are for $T = 0.1$, $N = 32 \times 32$ and n=0.1.

References

[1] S. Nakajima: Prog. Theor. Phys. **50** (1973) 1101.

[2] P. W. Anderson and W. F. Brinkman: Phys. Rev. Lett. **30** (1973) 1108.

[3] W. F. Brinkman and P. W. Anderson: Phys. Rev. A **8** (1973) 2732.

[4] W. F. Brinkman, J. W. Serene and P. W. Anderson: Phys. Rev. A **10** (1974) 2786.

[5] Y. Kuroda: Prog. Theor. Phys. **51** (1974) 1269.

[6] C. P. Lusher, B. P. Cowan and J. Saunders: Phys. Rev. Lett. **67** (1991) 2497.

[7] S. R. White, D. J. Scalapino, R. L. Sugar, E. Y. Loh, J. E. Gubernatis and R. T. Scalettar: Phys. Rev.B 40 (1989) 506

[8] G. Baym and L. P. Kadanoff: Phys. Rev. **124** (1961) 287.

[9] N. E. Bickers and D. J. Scalapino: Annals of Physics. **193** (1989) 206.

[10] E.Y. Loh Jr and J.E. Gubernatis: in *Electronic Phase Transitions* (North-Holland, Amsterdam, 1992) eds. W. Hanke and Yu. V. Kopaev.

[11] *Numerical Recipes* (Press Syndicate of the University of Cambridge, New York, 1986) eds. W. H. Press, B. P. Flannery, S. A. Teukolsky and W. T. Vetterling.

[12] K. Maki: Prog. Theor. Phys. **39** 897 (1968).

[13] R. S. Thompson: Phys. Rev. B **1** 327 (1970).

[14] L. G. Aslamasov and A. I. Larkin: Phys. Lett. **26** A 238 (1968).

[15] In the 2D Hubbard model near the half filled case, $n \sim 1$, the contributions of the AL diagrams were also found to be small. See, N. E. Bickers, D. J. Scalapino and S. R. White: Phys. Rev. Lett. **62** 961 (1989); N. E. Bickers and S. R. White: Phys. Rev. **B43** 8044 (1991).

[16] D. S. Hirashima and H. Takahashi: J. Phys. Soc. Jpn. **67** (1998) 3816.

[17] H. J. Vidberg and J. W. Serene: J. Low. Temp. Phys **29** (1977) 179.

[18] M. A. Baranov and M. Yu. Kagan: Z. Phys. B **86** (1992) 237.

[19] M. A. Baranov, A. V. Chubukov and M. Yu. Kagan: Int. J. Mod. Phys. B **6** (1992) 2471.

[20] A.V. Chubukov: Phys. Rev. B **48** (1993) 1097.

[21] S. Ohnishi and K. Miyake: J. Phys. Soc. Jpn. **68** (1999) 3927.

[22] This is brought to the author's attention by K. Miyake.

[23] A. B. Migdal: Soviet Phys. JETP. **1** (1958) 996.